THE JOURNAL OF BIOLOGICAL CHEMISTRY VOL. 281, NO. 21, pp. 14918–14926, May 26, 2006

The X-ray Crystal Structures of Human α-Phosphomannomutase 1 Reveal the Structural Basis of Congenital Disorder of Glycosylation Type 1a*

Received for publication, February 16, 2006, and in revised form, March 8, 2006 Published, JBC Papers in Press, March 15, 2006, DOI 10.1074/jbc.M601505200

Nicholas R. Silvaggi[‡], Chunchun Zhang[§], Zhibing Lu[‡], Jianying Dai[§], Debra Dunaway-Mariano[§], and Karen N. Allen[‡1]

From the [‡]Department of Physiology and Biophysics, Boston University School of Medicine, Boston, Massachusetts 02118 and the [§]Department of Chemistry, University of New Mexico, Albuquerque, New Mexico 87103-0001

Congential disorder of glycosylation type 1a (CDG-1a) is a congenital disease characterized by severe defects in nervous system development. It is caused by mutations in α-phosphomannomutase (of which there are two isozymes, α-PMM1 and α-PPM2). Here we report the x-ray crystal structures of human α-PMM1 in the open conformation, with and without the bound substrate, α-D-mannose 1-phosphate. α-PMM1, like most haloalkanoic acid dehalogenase superfamily (HADSF) members, consists of two domains, the cap and core, which open to bind substrate and then close to provide a solvent-exclusive environment for catalysis. The substrate phosphate group is observed at a positively charged site of the cap domain, rather than at the core domain phosphoryl-transfer site defined by the Asp^{19} nucleophile and Mg^{2+} cofactor. This suggests that substrate binds first to the cap and then is swept into the active site upon cap closure. The orientation of the acid/base residue Asp^{21} suggests that α-phosphomannomutase (α-PMM) uses a different method of protecting the aspartylphosphate from hydrolysis than the HADSF member β-phosphoglucomutase. It is hypothesized that the electrostatic repulsion of positive charges at the interface of the cap and core domains stabilizes α-PMM1 in the open conformation and that the negatively charged substrate binds to the cap, thereby facilitating its closure over the core domain. The two isozymes, α-PMM1 and α-PMM2, are shown to have a conserved active-site structure and to display similar kinetic properties. Analysis of the known mutation sites in the context of the structures reveals the genotype-phenotype relationship underlying CDG-1a.

Glycoproteins play fundamental roles in humans (1, 2) where they are active in cell recognition and adhesion, development, and homeostasis (3–7). Defects in protein glycosylation lead to a variety of disease states known collectively as congenital disorders of glycosylation (CDG).[2] The most common CDG, congenital disorder of glycosylation type 1a (CDG-1a) (8), manifests in infancy with physical and developmental abnormalities. Numerous clinical genotypes have been identified, with the range of phenotypes extending from mild to severe (9, 10). CDG-1a is caused by mutations in the gene encoding α-phosphomannomutase (α-PMM) (11–13). The most common mutant, R141H (40% of disease alleles of CDG-1a patients), has a high carrier frequency of 1/70 in the general population. Individuals homozygous for this mutation have not been identified, suggesting that this genotype is lethal (12).

Human α-PMM, which catalyzes the conversion of D-mannose 6-phosphate (Man-6-P) to α-D-mannose 1-phosphate (α-Man-1-P) (see Fig. 1) is required for GDP-mannose and dolichol-phosphate-mannose biosynthesis. Two isoforms are found; PMM2 is expressed in all tissues, whereas expression of PPM1 (65% sequence identity with PMM2) is restricted to the brain and lungs (14). α-PMM belongs to the haloalkanoic acid dehalogenase superfamily (HADSF), distinguishing it both structurally and mechanistically from the phosphomanno/phosphoglucomutase enzymes of the phosphohexomutase superfamily that are integral to glycolysis in prokaryotes and eukaryotes (15) and to alginate biosynthesis in Gram-negative bacteria (16).

Within the HADSF, α-PMM is distinguished from the bacterial β-phosphoglucomutase (β-PGM) in its C(1) anomer specificity as well as in the position and fold of the cap domain which serves as a lid over the conserved catalytic core domain. In HADSF members, wherein phosphatases predominate, the conserved aspartate nucleophile of the core domain mediates the transfer of the phosphoryl group. Remarkably, the α-PMM and β-PGM evolved independently to arrive at an adaptation of the phosphatase scaffold, which allows the aspartylphosphate of the core domain to discriminate between solvent and the sugar-phosphate substrate as the phosphoryl group acceptor.

Herein we report the x-ray crystallographic structures of α-PMM1 in the Mg^{2+}-bound form and in complex with the substrate of the reaction, α-Man-1-P. These structures are analyzed in the context of the coordinates for uncomplexed α-PMM2 deposited in the Protein Data Bank by the Center for Eukaryotic Structural Genomics (accession code 2AMY) to identify active-site residues with roles in binding and catalysis as well as residues involved in subunit dimerization. The structure and kinetic analyses of α-PMM1 and α-PMM2 provide for the first time insight into how quaternary structure, stability, and catalytic efficiency are altered in clinically important mutants.

EXPERIMENTAL PROCEDURES

Materials—Except where indicated, all chemicals were obtained from Sigma. Primers, T4 DNA ligase, and restriction enzymes were from Invitrogen. The Geneclean spin kit and the Qiaprep spin miniprep kit were from Qiagen. Host cells were purchased from Novagen. The Biolmol green phosphate assay kit was purchased from Biolmol

* This work was supported by Grant GM61099 from the National Institutes of Health (NIH) (to K. N. A. and D. D.-M.) and NIH Training Grant HL07291 (to N. R. S.). The costs of publication of this article were defrayed in part by the payment of page charges. This article must therefore be hereby marked "*advertisement*" in accordance with 18 U.S.C. Section 1734 solely to indicate this fact.

The atomic coordinates and structure factors (code 2FUC and 2FUE) have been deposited in the Protein Data Bank, Research Collaboratory for Structural Bioinformatics, Rutgers University, New Brunswick, NJ (http://www.rcsb.org/).

[1] To whom correspondence should be addressed: 715 Albany St., R-702, Boston, MA 02118. Tel.: 617-638-4398; Fax: 617-638-4273; E-mail: allen@med-xtal.bu.edu.

[2] The abbreviations used are: CDG, congenital disorders of glycosylation; CDG-1a, congenital disorder of glycosylation type 1a; α-PMM, α-phosphomannomutase; α-Man-1-P, α-D-mannose 1-phosphate; HADSF, haloalkanoic acid dehalogenase superfamily; β-PGM, β-phosphoglucomutase, α-PMM1·Man-1-P, α-PMM1 in complex with α-D-mannose 1-phosphate; SeMet, selenomethionine; DTT, dithiothreitol.

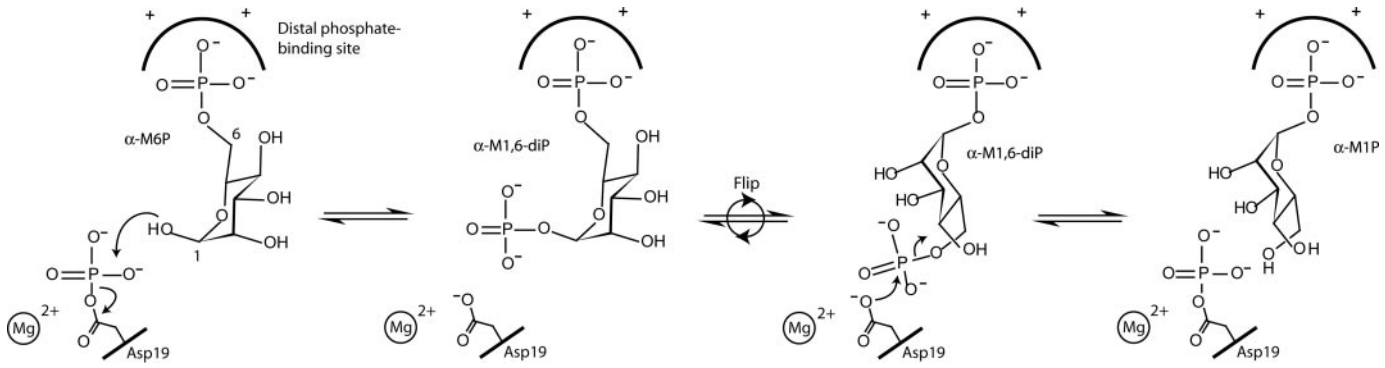

FIGURE 1. **Scheme for the reaction catalyzed by human α-phosphomannomutase.** The C-1 and C-6 positions on the hexose ring are labeled in the first step.

Research Laboratories Inc. The α-mannose 1,6-bisphosphate used in the kinetic assays was prepared according to published procedure (13).

Cloning, Expression, and Purification—The cDNA encoding the α-PMM1 gene was purified from the host cells purchased from ATCC (ATCC 7483527). Oligonucleotide primers (5′-CGCGGACCTG-CAGCCATGGCA, and 5′-ACACACAGATGTGGGATCCGGTCA), containing the restriction endonuclease cleavage sites NcoI and BamHI (underlined), were used to amplify the α-PMM1 open reading frame. The open reading frame of α-PMM2 was obtained from the Mammalian Genome Collection, *Homo sapiens*, and amplified using primers containing NdeI and a BamHI restriction sites (underlined) (5′-GAAACTGGGCATATGGCAGCGCCT-3′ and 5′-TGTGGGAG-GATCCTCGGCTCT-3′). The α-PMM1 and α-PMM2 genes were cloned into pET-28b(+) or pET-23b(+) vectors (Stratagene), respectively. The ligation products (pET-28b(+)-pmm1 or pET-23b(+)-pmm2) were used to transform *Escherichia coli* JM109 competent cells. The purified plasmids were sequenced by the Tufts University Core Facility.

α-PMM-1 was purified from *E. coli* Rosetta™ (DE3) cells containing the pET-28b(+)-pmm1 plasmid. Transformed cells (4L) were grown at 37 °C in Luria broth (or minimal medium containing selenomethionine) containing 50 μg/ml ampicillin and induced for 4 h with 0.4 mM isopropyl β-D-thiogalactopyranoside. Cells were harvested by centrifugation and the pellet (11 g) was suspended in 100 ml of ice-cold lysis buffer (50 mM Hepes, pH 7.5, 5 mM DTT). Cells were lysed by sonication (6 × 6 min at 50% power and 30% duty cycle) with a Branson sonifier 250 (VWR Scientific Inc.). The cell lysate was centrifuged at 4 °C for 60 min at 18,000 rpm (38,384 × *g*). The protein precipitated with 40–50% $(NH_4)_2SO_4$ was harvested by centrifugation at 15,000 rpm (26,895 × *g*) for 15 min. Following dissolution in 25 ml of lysis buffer and dialysis against buffer A (50 mM Hepes, pH 7.5, 0.5 mM DTT) overnight, the protein was loaded onto a 100-ml DEAE-Sepharose column (Amersham Biosciences) pre-equilibrated with buffer A. The column was washed with 100 ml of buffer A, and eluted with a 0.7-liter linear gradient of 0–0.5 M NaCl in buffer A. Fractions containing α-PMM1 were combined and $(NH_4)_2SO_4$ was added to 1 M. The solution was centrifuged at 15,000 rpm (26,895 × *g*) for 5 min to remove precipitated protein. The supernatant was loaded onto a 25-ml butyl-Sepharose column (Amersham Biosciences) pre-equilibrated with 1 M $(NH_4)_2SO_4$ in buffer A. The column was washed with 50 ml 1 M $(NH_4)_2SO_4$ in buffer A and then eluted with a 200-ml linear gradient of 1 to 0 M $(NH_4)_2SO_4$ in buffer A. α-PMM1 was concentrated and stored at −80 °C. The protein, shown to be >95% pure by SDS-PAGE, was obtained in a yield of 2 mg of protein/g of cell paste.

Selenomethionine-substituted α-PMM1 was expressed in *E. coli* BL21-CodonPlus cells. The cells were grown in minimal medium prepared by mixing 200 ml of 20× M9 (10 g of NH_4Cl, 30 g of KH_2PO_4, 60 g of Na_2HPO_4, 500 ml of H_2O, pH 7.5), 20 ml of amino acid mix I (the 20 standard amino acids excluding Met, Tyr, Trp, and Phe, each at 4 mg/ml), 40 ml of amino acid mix II (Tyr, Trp, and Phe, each at 2 mg/ml in distilled/deionized H_2O, pH 9.0), 1 ml of vitamin mixture (riboflavin, niacinamide, pyridoxine monohydrochloride, and thiamine, each at 1 mg/ml), 4 ml of 1 M $MgSO_4$, 4 ml of 12.5 mg/ml $FeSO_4$, 20 ml of 40% (w/w) glucose, and 4 ml of 10 mg/ml selenomethionine in a final volume of 2 liters. Chloramphenicol (16.5 mg/liter) and kanamycin (50 mg/liter) were added to the culture. The culture was grown at 30 °C with shaking at 200 rpm until the A_{600} reached 0.8–1.1 (24 h), at which point α-PMM1 expression was induced by adding IPTG to a final concentration of 0.4 mM. The cells were grown for an additional 10 h at 25 °C and harvested by centrifugation. The protein was purified using the procedure described above, except that the DTT concentration was increased to 10 mM, and 1 mM EDTA was added throughout.

The purification of α-PMM2 was similar to that of α-PMM1 with a few modifications. The cell pellet from a 10-liter culture of *E. coli* Rosetta™ (DE3) cells (30 g) containing the pET-23b(+)-pmm2 plasmid was suspended in 300 ml of Tris-HCl buffer (pH 8.5, 10 mM $MgCl_2$, 5 mM DTT). The cell lysate was loaded directly onto a Q-Sepharose column (Amersham Biosciences), pre-equilibrated with Tris-HCl buffer (pH 8.5, 10 mM $MgCl_2$, 1 mM DTT). The fractions containing α-PMM2 were pooled, and $(NH_4)_2SO_4$ was added to 15%. The fractions were then loaded onto a phenyl-Sepharose column (Amersham Biosciences), pre-equilibrated with Tris-HCl buffer containing 15% $(NH_4)_2SO_4$. The protein was eluted with a 600-ml 15% to 0% $(NH_4)_2SO_4$ gradient. The fractions having α-PMM activity were pooled and concentrated, then dialyzed against 50 mM Hepes, pH 7.2, 5 mM $MgCl_2$, 1 mM DTT at 4 °C.

Crystallization and Data Collection—Crystals of SeMet α-PMM1 were grown by the hanging-drop vapor-diffusion method over well solution containing 15–18% polyethylene glycol 3350, 0.15 M DL-malate, pH 7.0, 50 mM $MgCL_2$, and 8 mM 2-mercaptoethanol. Drops were formed by mixing 2 μl of protein solution (10 mM Hepes, pH 7.5, 100 mM NaCl, 5 mM $MgCl_2$) at 15–25 mg/ml with 2 μl of well solution. Crystals were transferred to paratone N and flash-cooled in a gaseous N_2 stream at 100 K. X-ray diffraction data were collected at the National Synchrotron Light Source, Beamline X12C. α-PMM1 crystallized in space group $P4_32_12$ with unit cell dimensions $a = b = 50.9$ Å, $c = 213.0$ Å. The 0.7 × 0.3 × 0.3-mm crystal diffracted to 2.1 Å resolution. The ligand-bound structure was obtained by soaking SeMet α-PMM1 crystals for 1 h in mother liquor containing 100 mM α-D(+)-mannose 1-phosphate. All data sets were indexed and scaled using DENZO and SCALEPACK (17).

TABLE 1
Data collection and refinement statistics

	SeMet αPMM1			
	Edge	Inflection point	Remote	α-Man-1-P-bound
Resolution (Å) (last shell)[a]	50.0–2.10 (2.18–2.10)			50.0–1.75 (1.81–1.75)
Wavelength (Å)	0.9797	0.9794	0.9500	1.1000
Space group	$P4_32_12$			$P4_32_12$
Cell dimensions (Å)	$a = b = 51.7$, $c = 216.0$			$a = b = 51.4$, $c = 214.7$
Reflections				
Observed	339,621	337,677	337,985	393,048
Unique	17,978	17,984	18,017	28,735
Completeness (%)[a]	99.0 (99.0)	99.1 (99.0)	99.1 (99.0)	94.8 (75.5)
R_{merge} **(%)**[a,b]	5.6 (40.5)	6.4 (44.8)	6.5 (49.4)	5.0 (45.5)
$I/\sigma(I)$[a]	45.3 (8.8)	44.5 (7.9)	43.4 (7.5)	42.4 (4.0)
f'/f'' **(e^-)**	−7.0/3.5	−6.0/5.0	−3.0/2.5	
Figure of merit (%)	61.7			

Refinement statistics		
	Native	α-Man-1-P-bound
No. of protein/water atoms per asu	1,971/171	1,987/235
Number of reflections (work/free)	14,980/868	25,766/1,464
R_{work}/R_{free} **(%)**	19.1/20.6	20.5/24.1
Average *B*-factor (Å2)		
Protein atoms	34.1	31.2
α-D-Mannose 1-phosphate	na	28.9
Mg(II) ions	27.9	27.0
Water	43.8	42.9
Root mean square deviations		
Bond lengths (Å)	0.009	0.008
Bond angles (°)	1.22	1.17

[a] Values in parentheses apply to the high resolution shell indicated in the resolution row.
[b] $r = \Sigma(I - \langle I \rangle)^2/\Sigma I^2$.

Structure Determination and Model Refinement—Because structure determination by molecular replacement was unsuccessful, the structure was phased by the multiple wavelength anomalous diffraction method, using three 2.1 Å SeMet data sets. The selenium substructure was solved using BnP (18), which found three of the four selenium sites in the protein. The sites were confirmed by comparison with the anomalous difference Patterson map. The N-terminal methionine, along with the next 10 residues, was disordered. An initial model was built using RESOLVE (19) and improved by manual rebuilding in the graphics suite COOT (20). This partial model was refined in the REFMAC5 (21) module of the CCP4 suite (22) using the Hendrickson-Lattman coefficients from BnP. Electron density maps calculated from the combined phases were of very high quality and permitted rapid rebuilding of the model. Iterative cycles of restrained refinement in REFMAC5 and rebuilding in COOT ultimately yielded a model containing 244 of 262 residues, 171 water molecules, and 2 Mg^{2+} ions. The quality of the model at this point was assessed by MOLPROBITY (23), and 235 residues (96.3%) were in the favored regions, 9 residues were in the additionally allowed regions, and no residues were in the disallowed regions.

The ligand-bound structure was solved by Fourier difference methods using phases from the 2.1 Å SeMet native model. After rigid body refinement in REFMAC5 the electron density for Man-1-P was clearly defined. The Man-1-P was not modeled until the model reached an R_{work} of 22.3% and an R_{free} of 27.4%. After several more rounds of model building and refinement, the final α-PMM1·Man-1-P model was comprised of residues 13–258 of α-PMM1, 235 water molecules, two Mg^{2+} ions, and one molecule of Man-1-P. Data collection and refinement statistics for both models are reported in Table 1.

Steady-state Kinetics—All 1-ml kinetic assays were carried out at 25 °C in 50 mM K^+Hepes, pH 6.5, containing 10 mM $MgCl_2$. The initial velocity of α-PMM catalyzed Glc-6-P formation from α-Glc-1-P was measured in the presence of 50 μM α-Glc-1,6-bisP, 0.2 mM NADP, and 5 units/ml Glc-6-P dehydrogenase by monitoring the increase in absorbance at 340 nm ($\Delta\epsilon = 6.2\ mM^{-1}\ cm^{-1}$) resulting from the Glc-6-P dehydrogenase catalyzed reduction of NADP. The initial velocity of α-PMM-catalyzed Man-6-P formation from α-Man-1-P was measured in the presence of 50 μM α-Man-1,6-bisP (13), 5 units/ml glucose-6-phosphate dehydrogenase, 5 units/ml phosphomannose isomerase, 5 units/ml phosphoglucose isomerase by monitoring the increase in absorbance at 340 nm ($\Delta\epsilon = 6.2\ mM^{-1}\ cm^{-1}$) resulting from the Glc-6-P dehydrogenase-catalyzed reduction of NADP. The k_{cat} and K_m values were determined from the initial velocity data using the equation $V_0 = V_m[A]/(K_m + [A])$, where $[A]$ is the α-Glc-1-P or α-Man-1-P concentration, V_0 is the initial velocity, V_m is the maximum velocity, and K_m is the Michaelis constant. The k_{cat} was calculated from the ratio of V_{max} and the α-PMM concentration.

RESULTS AND DISCUSSION

Overall Structure—Recombinant human α-PMM1 was purified by conventional chromatographic techniques and crystallized from a solution of polyethylene glycol 3350, $MgCl_2$, β-mercaptoethanol, and DL-malic acid at pH 7.0 for x-ray structure determination. Both the native and SeMet α-PMM1 crystallized in space group $P4_32_12$ (unit cell dimensions $a = b = 50.9$ Å, $c = 213.0$ Å) with one molecule in the asymmetric unit. Molecular replacement using the structure of α-PMM2 (65% identical, Protein Data Bank accession code 2AMY, unpublished submission by the Center for Eukaryotic Structural Genomics) as the search model did yield a viable solution; however, the resulting model did not refine well, and several surface loops appeared to be disordered. To obtain experimental phases, the structure was

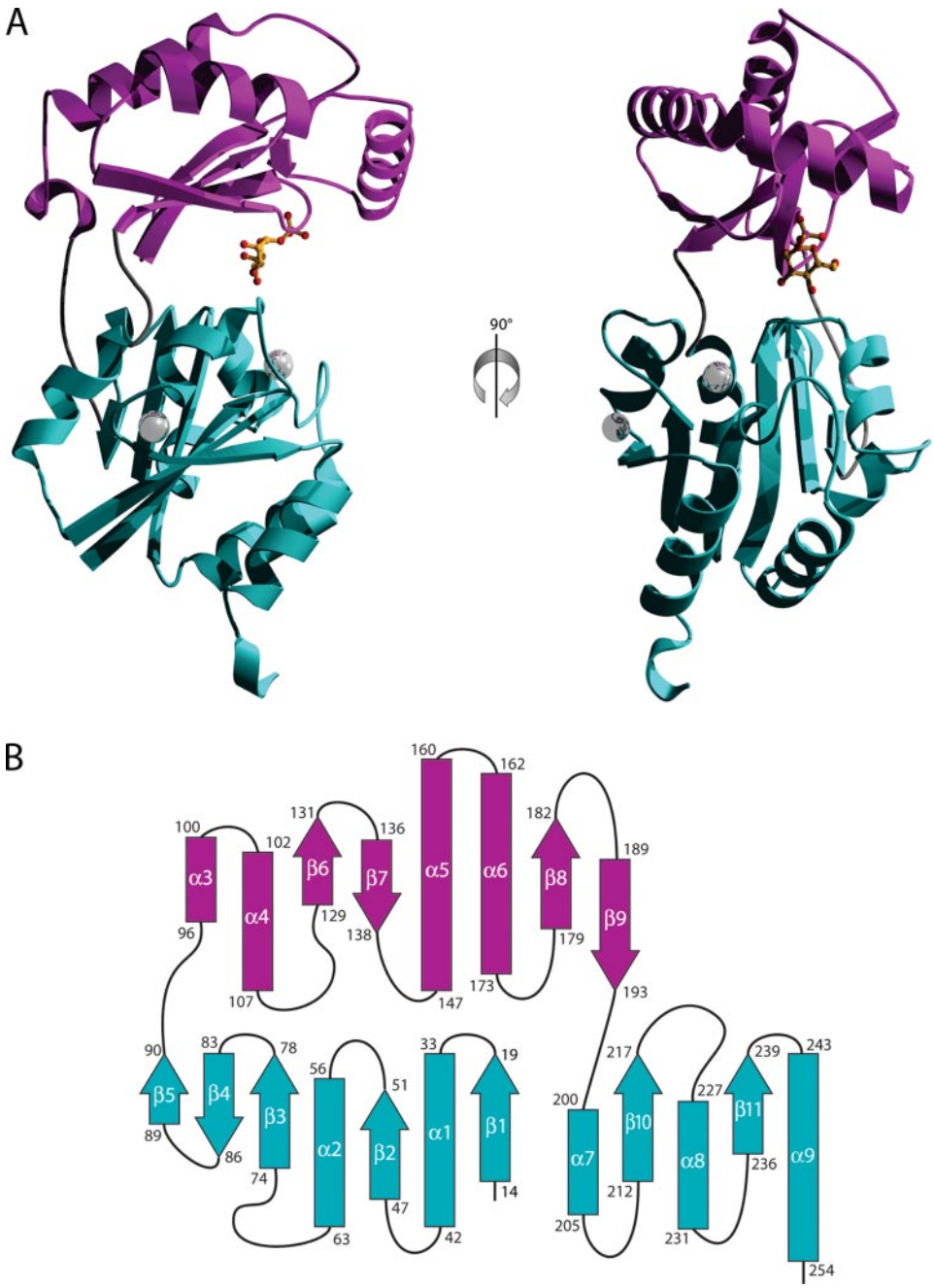

FIGURE 2. *A*, structure of human α-phosphomannomutase complexed with α-D-mannose 1-phosphate. The cap domain is *magenta* and the core domain *cyan*. Man-1-P is shown as *ball-and-stick* (*orange*) and the two Mg^{2+} ions as *metallic spheres*. The image was rendered using MOLSCRIPT (38) and POVRAY. *B*, schematic representation of the arrangement of secondary structure elements in α-PMM1 core (*cyan*) and cap (*magenta*).

determined using multiple wavelength anomalous diffraction phasing of the selenomethionine-substituted protein. The final model contained 245 of 262 residues. The first 11 residues at the N terminus and the last 6 residues at the C terminus were disordered. The refined model of the Mg^{2+}-bound form of α-PMM1 was used to phase the structure of α-PMM1 in complex with α-D-mannose 1-phosphate (α-PMM1·Man-1-P) obtained by soaking the Mg^{2+}-bound crystals with α-Man-1-P.

α-PMM1, like other HADSF phosphotransferases, is comprised of two domains, a core domain and a smaller cap domain (Fig. 2). The overall dimensions of the monomer are ~63 × 31 × 42 Å. The core domain (residues 1–90 and 198–262) consists of a six-stranded parallel β-sheet (β1–β5 and β10-β11) flanked by five α-helices (α1-α2 and α7–α9) (Fig. 2*B*) with typical β-α-β connections. The cap domain (residues 95–194) is inserted between β5 and α7 of the core domain. The αββ(α)αββ topology of the cap domain, as well as its position in the primary sequence between motifs 2 and 3 (see Ref. 24 for review), place this enzyme in subclass IIb of the HADSF. The secondary structure elements are arranged to form a four-stranded antiparallel β-sheet (β6-β7 and β8-β9) topped by three α-helices (α4–α6). Two flexible "hinge" regions comprising residues 91–94 and 195–197 connect the two domains. The hinge regions were identified using visual inspection of the structure together with the program FlexOracle (25). In both structures reported herein, the cap domain is in an open conformation, with the active site exposed to solvent.

The 29.7-kDa monomer forms a homodimer in solution as demonstrated by size-filtration chromatography. This dimer is observed in the crystal structure of α-PMM1, with the interface consisting exclusively of interactions between the cap domains (Fig. 3*A*). Two major interactions dominate the dimer interface: a helix-helix interaction between the first α-helices (α4) and an antiparallel β-sheet interaction between

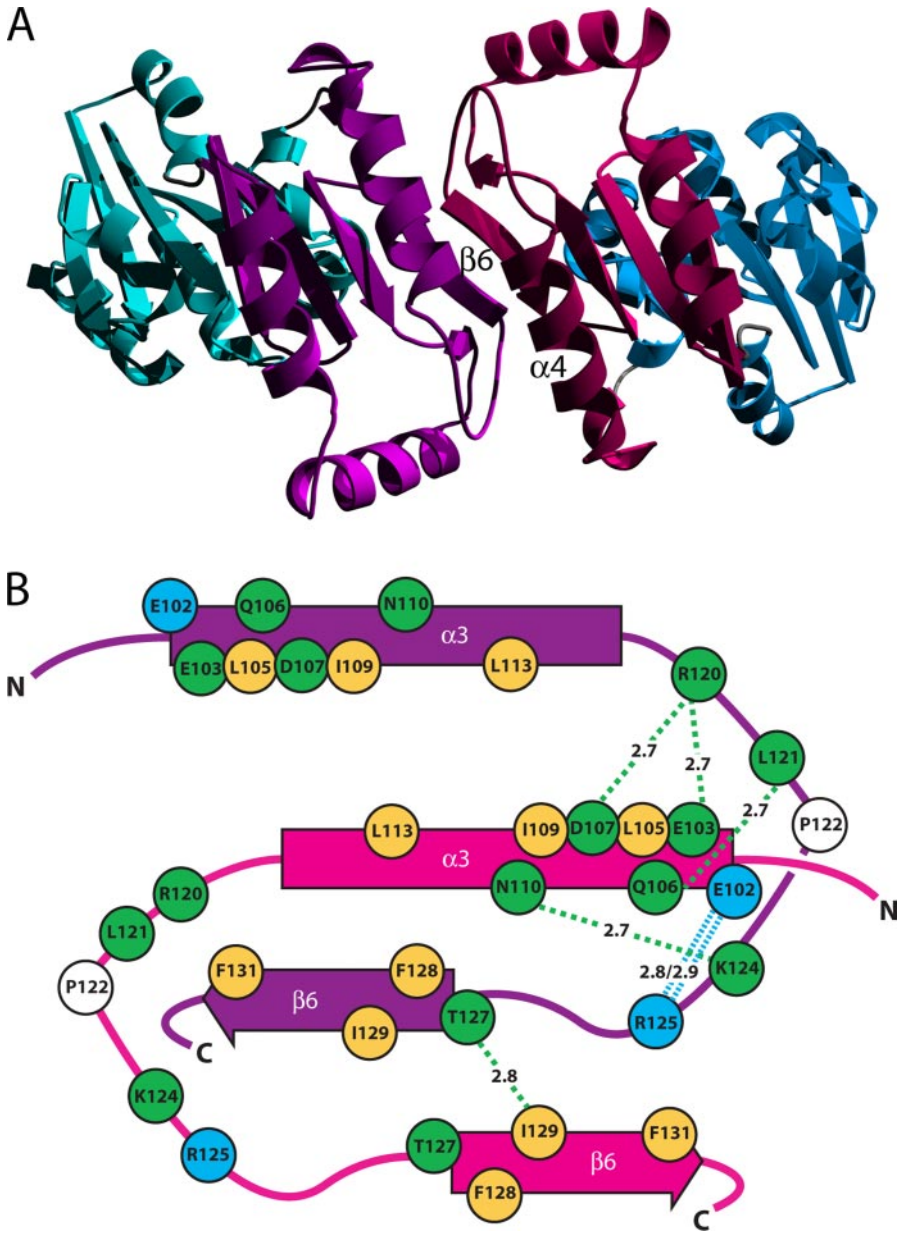

FIGURE 3. *A*, *ribbon* representation of the α-PMM1 dimer. The molecule has been rotated 90° on the horizontal axis relative to Fig. 2. The cap and core domains of monomer A are *magenta* and *cyan*, respectively, while the cap and core of monomer B are *red* and *blue*, respectively. The image was rendered using MOLSCRIPT (38) and POVRAY. *B*, schematic representation of the interactions between monomers at the dimer interface. For clarity, the distances are shown for only the right half of the dimer interface. *Green circles* denote residues involved in hydrogen bonds, *blue circles* denote residues involved in salt bridges, and *yellow circles* denote residues forming the hydrophobic core of the interface. Pro[122], which imparts a kinked turn necessary for positioning Arg[125], is shown as a *white circle*.

the first β-strands (β6) of the two cap domains. The interaction between the strands creates an extended eight-stranded β-sheet across the two monomers, holding the two core domains away from one another. Residues Leu[105], Ile[109], Leu[113], Phe[128], Ile[129], and Phe[131] form a hydrophobic core at the dimer interface. Several hydrogen bonds and a salt bridge anchor the interface at each end (Fig. 3*B*). The same oligomerization interface can be observed in the structure of human α-PMM2, demonstrating that this is a conserved feature of human α-PMMs. One of the more common deleterious mutations of α-PMM2, F119L (Phe[128] in α-PMM1), is located in the center of the dimer interface (Fig. 3*B*), highlighting the potential importance of the quaternary structure for function and/or stability of the protein.

Based on previous studies of catalytic cycling in other HADSF enzymes, it is known that the cap domain must dissociate from the core domain to allow substrate to bind, then associate to seal the active site from aqueous solvent (26, 27). A portion of the cap domain that would contact the core domain in α-PMM carries a large number of positively charged residues (Figs. 4 and 5). These include the three conserved residues Arg[150], Arg[143], and Arg[132] in α-PMM1 and Arg[141], Arg[134], and Arg[123] in α-PMM2. One might expect that there would be complementary negatively charged residues on the surface of the core domain; however, the corresponding surface of the core retains an overall positive charge contributed by conserved residues Arg[28] and Lys[58] in α-PMM1 and Arg[21] and Lys[51] in α-PMM2. Thus, rather than acting as a "clasp" these two surfaces may act as an electrostatic wedge retaining the correct interdomain orientation. Indeed, the importance of these residues to protein function is highlighted by the fact that the mutation R141H (Arg[150] in α-PMM1) has been identified as one of the major deleterious polymorphic mutations of α-PMM2.

Enzyme Active Site—The active site of α-PMM1 is located at the interface of the cap and core domains (Fig. 4). By analogy to other HADSF phosphatases, the key active-site residues are the catalytic nucleophile Asp[19], the putative acid/base residue Asp[21] (contributed by motif 1), Ser[54], which helps position the phosphoryl group (contributed by motif 2), the salt bridge residue Lys[198] (contributed by motif 3), and the metal-binding residue Asp[218] (contributed by motif 4). In both the

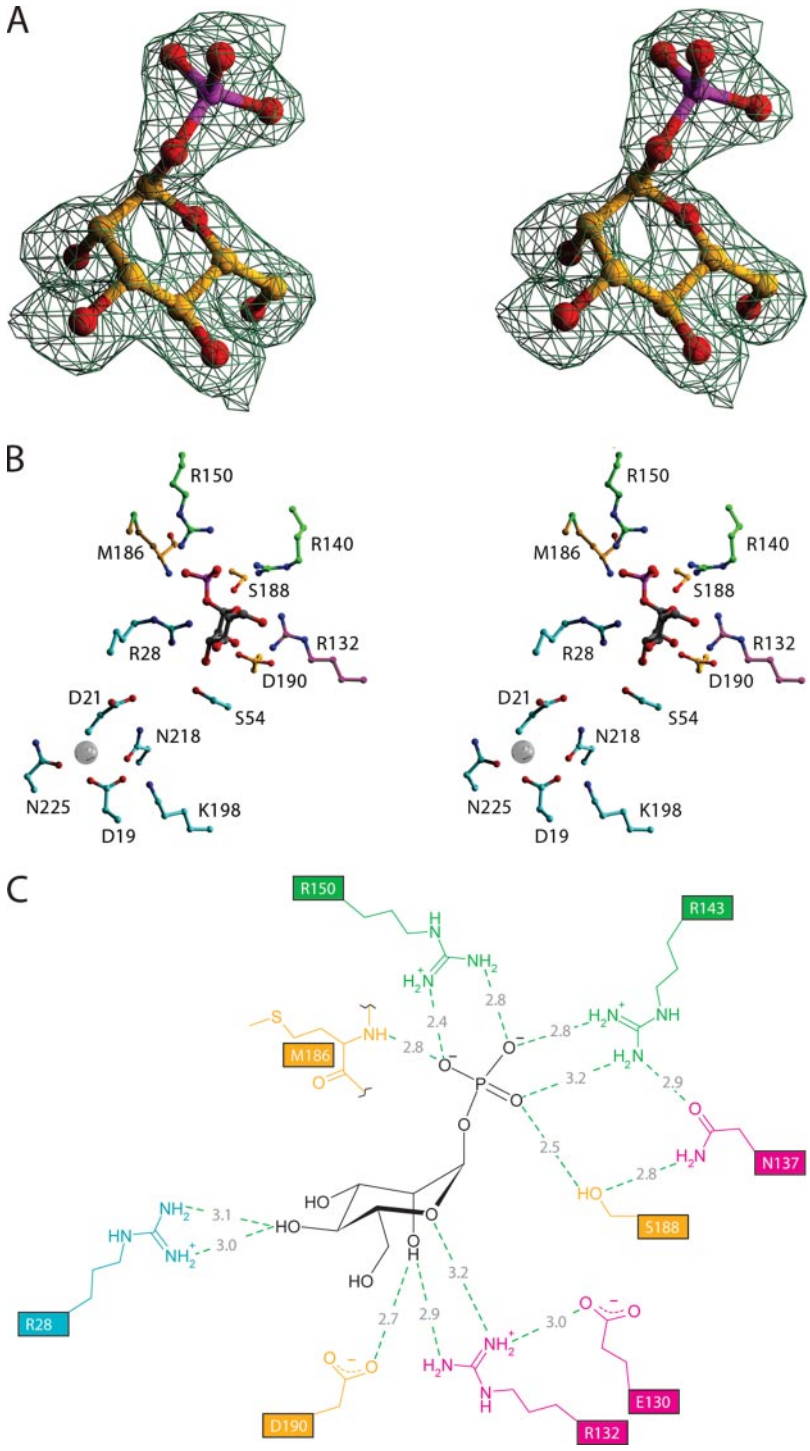

FIGURE 4. *A*, a stereo view of the α-D-mannose 1-phosphate moiety highlighting the well defined electron density for the ligand. The Man-1-P (*orange* carbon atoms) is shown as *ball-and-stick* with the $|F_o| - |F_c|$ omit electron density contoured at 3.0 σ (*green wire frame*). The image was rendered using MOLSCRIPT (38) and POVRAY. *B*, the enzyme active site with α-Man-1-P (*ball-and-stick* with *gray* carbons) bound. The core domain residues are shown with *cyan* carbon atoms, and cap domain residues have *magenta* carbons. Residues located in the primary substrate specificity loop are shown with *green* carbons, and those of the secondary substrate specificity loop have *orange* carbons. The Mg^{2+} ion is shown as a *metallic sphere*. The image was rendered using MOLSCRIPT (38) and POVRAY. *C*, schematic representation of the interactions between α-PMM1 and Man-1-P (*black*). The residues of the cap and core domains and the primary and secondary substrate specificity loops are colored as described for *B*. The distances of the interactions are given in Angstroms.

native and α-PMM1·Man-1-P structures, the acid/base residue Asp^{21}, stationed two residues upstream from the nucleophile (thus denoted the Asp-plus-2 residue), is held in position for proton transfer by a hydrogen bond to residue Gln^{62} contributed by α2, as has been noted previously for the corresponding residue in HADSF type IIA (28), type IIB (26), and type III (29) phosphatases. Because Asp^{21} is positioned to activate a water molecule as well as the C(6)OH of α-Man-1-P for attack at the aspartylphosphate, it is clear that a different mechanism for ensuring that phosphomutase activity predominates over phosphatase activity is operative in α-PMM than the substrate induced-fit mechanism, which is operative in β-PGM. In the case of β-PGM, the Asp general acid/base residue is pinned to the linker in the cap-open conformation and to the active site in the cap-closed conformation. The bound substrate and not a water molecule functions to stabilize the cap-closed conformation for catalytic turnover.

Substrate Binding—The structure of α-PMM1 with α-D-mannose 1-phosphate bound identifies the active-site residues contributing to substrate specificity. Since this structure was obtained by soaking preformed crystals of α-PMM1 with Man-1-P, the domain motions required to close the active site could not occur, because the enzyme conformation was held fast by the crystal lattice. The Man-1-P-bound structure was surprising because it was anticipated from observations of

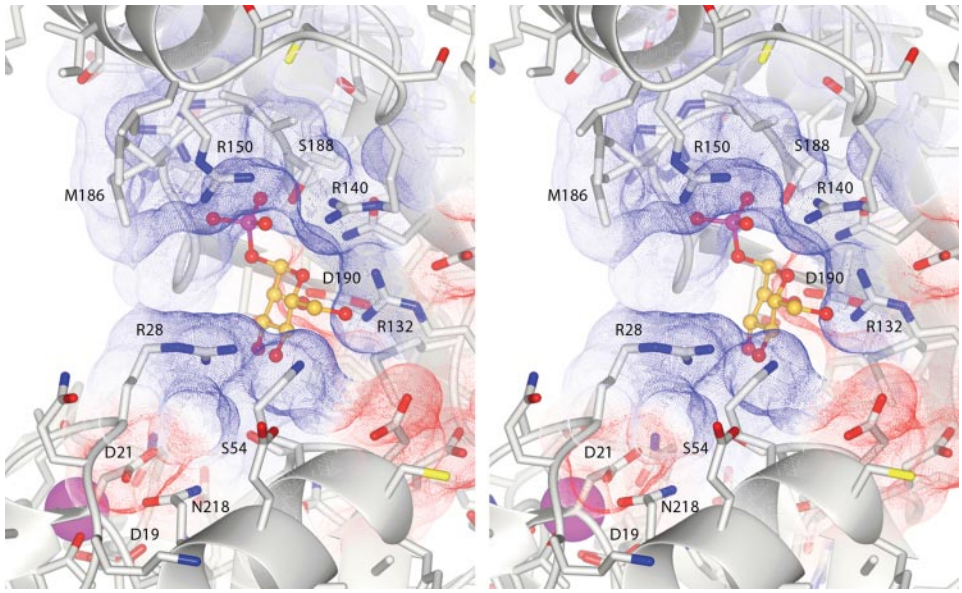

FIGURE 5. **The enzyme active site with Man-1-P (*orange ball-and-stick*) bound.** A *dot* surface shows the overall charge of the cap and core domain surfaces at the Man-1-P-binding site. The image was rendered using CCP4MG (39).

phosphate (and phosphate analog) binding to other HADSF members that the electropositive environment created by the active-site Ser^{54}, Lys^{198}, and Mg^{2+} would constitute a more competent phosphate-binding site than that of the cap domain (26, 27, 30). Thus, α-PMM1 is unique in that the phosphorylated substrate is seen bound primarily by interactions with the cap domain (Figs. 2*A* and 4). The electron density corresponding to the ligand was observed at 3.0σ in a $|F_o| - |F_c|$ electron density map (Fig. 4*A*). The α-PMM1·Man-1-P structure can be said to represent a collision complex, the first encounter of enzyme and substrate, and not the Michaelis complex immediately preceding the first chemical step. Indeed, if the intermediate α-mannose 1,6-(bis)phosphate is overlaid with the Man-1-P substrate in the α-PMM1·Man-1-P complex, the C(6)-phosphate group is 10 Å from the Asp^{19} nucleophile (that is, there is no phosphate group in the phosphoryl-transfer site). The implication of this observation is that substrate initially binds to the cap and not the core domain portion of the active site. Once the substrate is bound, there is presumably a change in the conformation of the hinge region that pushes the substrate into the active site as the cap binds to the core domain.

The surfaces of both domains at the Man-1-P-binding site carry an overall positive charge (Fig. 5). The residues constituting the Man-1-P-binding site are positioned on two loops of the cap domain, termed the primary (residues 140–162) and secondary (residues 181–190) substrate specificity loops. The corresponding loops have been described for BT4131, a homologous subclass IIb HADSF enzyme (26). α-PMM1 residues Arg^{143} and Arg^{150}, together with Ser^{188} and the main chain amide of Met^{186}, form the distal phosphate-binding site (Fig. 4, *B* and *C*). Other residues involved in Man-1-P binding are Asp^{190} and Arg^{132}, which hold the C-2 hydroxyl, and Arg^{28}, the sole core domain contact, which interacts with the C-4 hydroxyl. Although Arg^{132} is not part of either substrate specificity loop, it does directly contact the substrate. It is located on strand β6, which forms a major part of the dimer interface (see above) in both α-PMM1 and α-PMM2. The importance of this residue to substrate binding and its proximity to the dimer interface may explain, at least in part, the loss of activity observed when dimerization is disrupted by genetic mutation.

A Proposal for the Mechanism of Selective Phosphoryl Transfer—α-PMM, like β-phosphoglucomutase, catalyzes the interconversion of the hexose 1-phosphate and hexose 6-phosphate via a hexose-1,6-(bis)phosphate intermediate generated by reaction with the phosphoenzyme (Fig. 1). For a HADSF enzyme to act as a phosphotransferase, as opposed to a phosphatase, the active site of the phosphorylated enzyme must be capable of discriminating between the substrate and water as the phosphoryl group acceptor. In both subfamily I and subfamily II HADSF enzymes, the cap domain closes on the active site, sealing it from solvent (31, 32). In unliganded β-phosphoglucomutase, the Asp^{10} acid/base is involved in hydrogen bond interactions with the main chain amides of two residues in the flexible hinge region. In this orientation, the Asp^{10} acid/base is pointing away from the catalytic center, which prevents general base catalysis of phosphoryl transfer to water. Binding of substrate shifts the equilibrium between the open and closed forms of the enzyme, stabilizing the closed form. Upon cap closure, the β-phosphoglucomutase Asp^{10} acid/base rotates into the active site to form a hydrogen bond with the C(6)OH of the β-glucose 1-phosphate. In this way, catalysis is linked to cap closure.

The unliganded and the MIP-bound structures of α-PMM1 suggest a unique mechanism of discrimination between substrate and solvent. The Asp^{21} acid/base of α-PMM1 is engaged in a hydrogen bond with Gln^{62} (2.9 Å) located on helix α2 of the core domain. In the cap-open conformation, Asp^{21} is in position to function as an acid/base catalyst in the transfer of the phosphoryl group to and from the Asp^{19} nucleophile. Thus, solvent discrimination is not accomplished by coupling the positioning of the Asp^{21} acid/base catalyst with substrate induced cap closure. Rather, it must rely on transition-state stabilization by the unique active-site environment created in the cap-closed conformation. How, then, is substrate binding tied to cap closure? The α-PMM structures suggest that the positively charged surfaces at the interface of the cap and core domains (Fig. 5) observed in the unliganded enzyme may act as an electrostatic wedge. Binding of the negatively charged substrate would mitigate the electrostatic repulsion of the cap and core domains, favoring cap closure.

The Structural Effects of Clinically Observed Mutations—The correlation between mutation and α-PMM activity has been the object of only one study reported in 1999 by Pirard *et al.* (33). In this study, seven PPM2 mutants (D65Y, F119L, V129M, R141H, R162W, D188G, and V231M) were purified and their *in vitro* activity and thermal stability briefly surveyed. The R141H and D188G mutants proved to be the most catalytically impaired (0.4 and 2% of wild-type activity), correlating with the severity of the heterozygous R141H/D188G phenotype, while V231M proved to be the least stable at 40 °C. Although not biochemi-

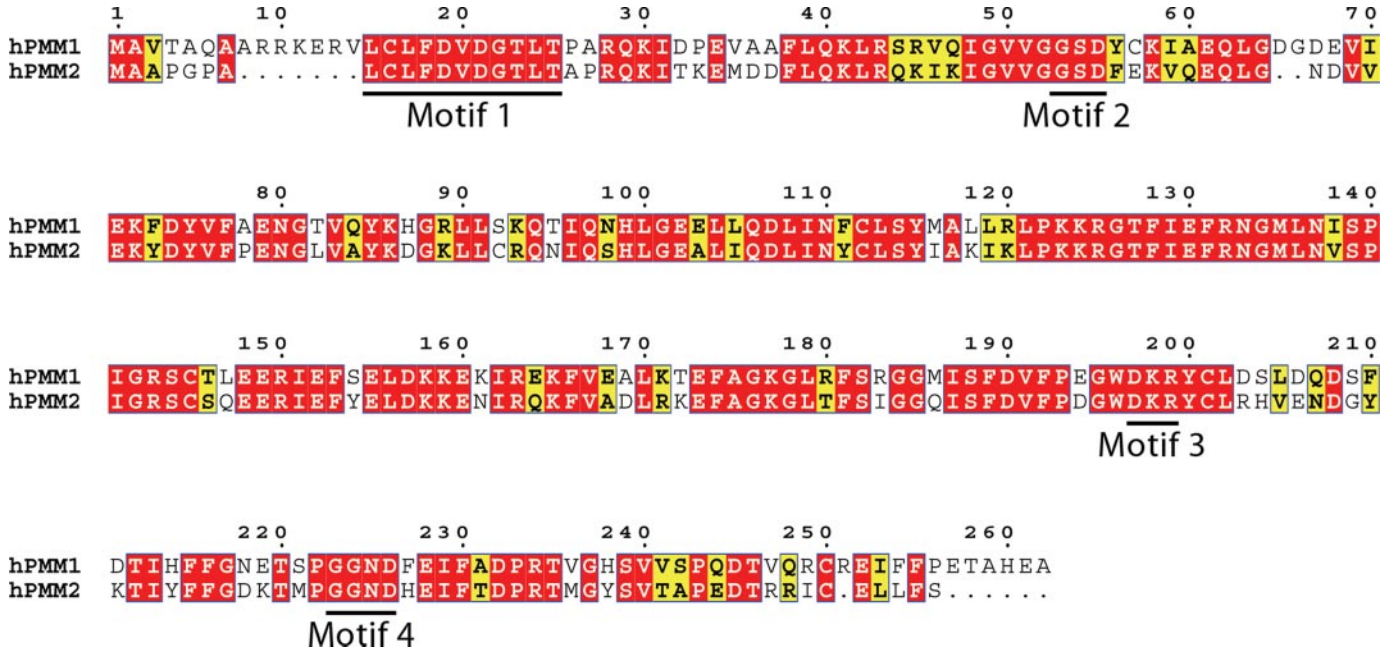

FIGURE 6. **Sequence alignment of human α-PMM1 and α-PMM2.** *Black bars* denote the four motifs of the HADSF. Identical residues are *boxed* in *red*, and conservative changes are *boxed* in *yellow*.

cally characterized to date, the R123G, F183S, and P113L mutations are nonetheless clinically significant (34, 35).

Because of its limited tissue distribution, mutations to α-PMM1 have not been linked to pathology. However, the PMM1 and PMM2 isozymes are quite similar (65% identical; Fig. 6), and the variable residues that are scattered throughout the structure are found mainly at the protein surface. The overall structures of α-PMM1 and α-PMM2 are very similar with root mean square deviations of 0.65 Å (for the cap) and 1.0 Å (for the core) when the two domains are overlaid separately. The dimer interface, active-site motifs (Fig. 6), and the hinge regions are conserved.

The numerous α-PMM2 mutation sites known to be associated with the CDG Type 1a phenotype are not localized to one particular region of the structure but are instead distributed throughout (Fig. 7). Based on their locations in the structure, the clinically important mutations can be classified on the basis of whether substrate binding and catalysis, dimerization, or protein stability are targeted. The most severe mutations, R141H (Arg^{150} in PMM1) and D188G (Asp^{197}) belong in the first category, as does R123G (Arg^{132}). As seen in the α-PMM1•Man-1-P structure, Arg^{150} (Arg^{141} in α-PMM2) is a crucial part of the distal phosphate-binding site, and loss of the positive charge at this location would impair substrate binding. This conclusion is in good agreement with the finding reported in Pirard *et al.* (14, 36) that the K_m for Man-1-P increased ~10-fold in the R141H mutant. The effect of the D188G (Asp^{197}) mutation is equally dramatic. This residue is adjacent to the motif 3 lysine, which is required for proper orientation of the nucleophilic aspartate. The R123G (Arg^{132}) mutation is also likely to effect substrate binding, because, as seen in the Man-1-P-bound structure, Arg^{132} of α-PMM1 makes direct interactions with the C-2 hydroxyl of Man-1-P. Of the mutations that appear to disrupt the dimer interface (F119L (Phe^{128}) and P113L (Pro^{122})), the F119L mutation would be expected to have the greatest ipmact, given that this residue is a major component of the hydrophobic core that comprises the dimer interface (Fig. 3*B*). The P113L mutation might alter the turn that positions Arg^{125} (Arg^{116} in α-PMM2) for formation of a salt bridge at the dimer interface.

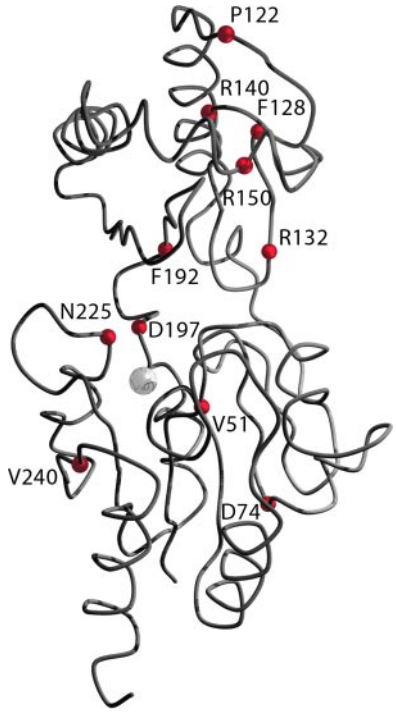

FIGURE 7. **Ribbon representation of the α-PMM1 structure showing the positions (Cα atoms) of the clinically relevant mutations (*red spheres*).**

The last category, mutations effecting folding and/or stability of the polypeptide, includes V129M (Ile^{138} in PMM1), V44A (Val^{51}), D65Y (Asp^{74}), and V231M (Val^{240}). These mutations occur in the interior of the cap or core domains (Fig. 7) and are therefore expected to be especially detrimental to native structure. Finally, one mutation, F183S (Phe^{192}) appears to be unique in that it may alter the interdomain motion required for catalysis. Phe^{183} is positioned at the start of the turn forming the second linker region, and it is possible that changes to this

TABLE 2

Steady-state kinetic constants

The steady-state kinetic constants measured for α-PMM1 and α-PMM2 catalyzed conversion of α-Glc-1-P to Glc-6-P (50 μM α-Glc-1,6-bisP cofactor) or α-Man-1-P to Man-6-P (50 μM α-Man-1,6-bisP cofactor) in solutions of 50 mM K^+Hepes, pH 6.5, 25 °C, containing 10 mM $MgCl_2$. The listed error was computed for the fit of the data set to equation 1. The value reported within the parentheses was reported earlier (14, 36) for reaction solutions containing 10 μM mannose-1,6-bisphosphate, 25 mM Hepes, pH 7.1, 30 °C, and 5 mM $MgCl_2$.

Substrate	Enzyme	k_{cat}	K_m	k_{cat}/K_m
		s^{-1}	μM	$M^{-1} s^{-1}$
α-Man-1-P	PMM1	4.39 ± 0.05(2.4)	54 ± 2(3.2)	8.1×10^4 (8×10^5)
α-Man-1-P	PMM2	3.9 ± 0.1 (2.4)	16 ± 2 (18)	2.5×10^5 (1.5×10^5)
α-Glc-1-P	PMM1	2.85 ± 0.06 (2.4)	7.5 ± 0.8 (5)	3.8×10^5 (5×10^5)
α-Glc-1-P	PMM2	1.72 ± 0.02 (0.1)	13.5 ± 0.4 (12)	1.3×10^5 (1×10^4)

residue interfere with the conformational changes expected to accompany substrate binding.

Kinetic Analysis—The structures of α-PMM1 and α-PMM2 are nearly identical, and the results of the kinetic assays reinforce this observation (Table 2). In addition, the kinetic analysis establishes the integrity of the recombinant PMM enzymes.

Both α-PMM1 and α-PMM2 are efficient catalysts with high specificity for glucose 1-phosphate and mannose 1-phosphate, as indicated by the magnitude of k_{cat}/K_m. In two instances the observed kinetic parameters differ significantly from those of previous studies (14, 36). First, the K_m of α-PMM1 for α-Man-1-P of 54 μM is larger than the published value of 3.2 μM. Nevertheless, this larger value is reasonable given that the average serum mannose concentration in humans is 55 μM (range 35–70 μM) (37). Also, Pirard *et al.* (14) reported that α-PMM2 is 10-fold more reactive with α-Man-1-P than with α-Glc-1-P, while our results indicate that there is no significant difference in reactivity, consistent with the conservation of active site residues.

Conclusion—The structural and kinetic analyses reported here in are important for several reasons. First, the key structural and functional sites in the two α-PMM isozymes are conserved. Thus, we anticipate that mutations will effect both enzymes in similar manner. The clinical manifestation, however, will depend on the isozyme tissue distribution. Second, location of the positions of the clinical mutations in the α-PMM structures provide a link between phenotype and genotype, which can be explored in detail through future structure/function analysis of the mutant enzymes. Finally, the divergence of mutase function in HASDF subclass II, which we contend is mechanistically distinct from that observed in the HASDF subclass I, provides a birds eye view of the diversity of nature at the molecular level.

Acknowledgments—We gratefully acknowledge the use of the data collection facilities at Beamline X12C of the National Synchrotron Light Source at Brookhaven National Laboratories.

REFERENCES

1. Varki, A. (1993) *Glycobiology* **3,** 97–130
2. Dwek, R. A. (1996) *Chem. Rev.* **96,** 683–720
3. Woods, R. J., Edge, C. J., and Dwek, R. A. (1994) *Nat. Struct. Biol.* **1,** 499–501
4. Rudd, P. M., Joao, H. C., Coghill, E., Fiten, P., Saunders, M. R., Opdenakker, G., and Dwek, R. A. (1994) *Biochemistry* **33,** 17–22
5. Rudd, P. M., Fortune, F., Patel, T., Parekh, R. B., Dwek, R. A., and Lehner, T. (1994) *Immunology* **83,** 99–106
6. Rademacher, T. W., Williams, P., and Dwek, R. A. (1994) *Proc. Natl. Acad. Sci. U. S. A.* **91,** 6123–6127
7. Brooks, S. A., Leathem, A. J., and Dwek, M. V. (1994) *Biochem. Soc. Trans.* **22,** 95S
8. Grunewald, S., Matthijs, G., and Jaeken, J. (2002) *Pediatr. Res.* **52,** 618–624
9. Neumann, L. M., von Moers, A., Kunze, J., Blankenstein, O., and Marquardt, T. (2003) *Eur. J. Pediatr* **162,** 710–713
10. Noelle, V., Knuepfer, M., Pulzer, F., Schuster, V., Siekmeyer, W., Matthijs, G., and Vogtmann, C. (2005) *Eur. J. Pediatr* **164,** 223–226
11. Matthijs, G., Schollen, E., Pardon, E., Veiga-Da-Cunha, M., Jaeken, J., Cassiman, J. J., and Van Schaftingen, E. (1997) *Nat. Genet.* **16,** 88–92
12. Matthijs, G., Schollen, E., Van Schaftingen, E., Cassiman, J. J., and Jaeken, J. (1998) *Am. J. Hum. Genet.* **62,** 542–550
13. Van Schaftingen, E., and Jaeken, J. (1995) *FEBS Lett.* **377,** 318–320
14. Pirard, M., Achouri, Y., Collet, J. F., Schollen, E., Matthijs, G., and Van Schaftingen, E. (1999) *Biochem. J.* **339,** 201–207
15. Dai, J. B., Liu, Y., Ray, W. J., Jr., and Konno, M. (1992) *J. Biol. Chem.* **267,** 6322–6337
16. Naught, L. E., and Tipton, P. A. (2001) *Arch. Biochem. Biophys.* **396,** 111–118
17. Otwinowski, Z., and Minor, W. (1997) *Methods Enzymol.* **276,** 307–326
18. Weeks, C. M., Blessing, R. H., Miller, R., Mungee, R., Potter, S. A., Rappleye, J., Smith, G. D., Xu, H., and Furey, W. (2002) *Z. Kristallogr.* **217,** 686–693
19. Terwilliger, T. C. (1999) *Acta Crystallogr. Sect. D Biol. Crystallogr.* **55,** 1863–1871
20. Emsley, P., and Cowtan, K. (2004) *Acta Crystallogr. Sect. D Biol. Crystallogr.* **60,** 2126–2132
21. Murshudov, G. N., Vagin, A. A., and Dodson, E. J. (1997) *Acta Crystallogr. Sect. D Biol. Crystallogr.* **53,** 240–255
22. Collaborative Computational Project, No. 4 (1994) *Acta Crystallogr. Sect. D Biol. Crystallogr.* **50,** 760–763
23. Davis, I. W., Murray, L. W., Richardson, J. S., and Richardson, D. C. (2004) *Nucleic Acids Res.* **32,** W615–W619
24. Allen, K. N., and Dunaway-Mariano, D. (2004) *Trends Biochem. Sci.* **29,** 495–503
25. Echols, N., Milburn, D., and Gerstein, M. (2003) *Nucleic Acids Res.* **31,** 478–482
26. Lu, Z., Dunaway-Mariano, D., and Allen, K. N. (2005) *Biochemistry* **44,** 8684–8696
27. Lahiri, S. D., Zhang, G., Dunaway-Mariano, D., and Allen, K. N. (2002) *Biochemistry* **41,** 8351–8359
28. Tremblay, L. W., Dunaway-Mariano, D., and Allen, K. N. (2006) *Biochemistry* **45,** 1183–1193
29. Peisach, E., Selengut, J., Dunaway-Mariano, D., and Allen, K. N. (2004) *Biochemistry* **43,** 12770–12779
30. Morais, M. C., Zhang, W., Baker, A. S., Zhang, G., Dunaway-Mariano, D., and Allen, K. N. (2000) *Biochemistry* **39,** 10385–10396
31. Wang, W., Cho, H. S., Kim, R., Jancarik, J., Yokota, H., Nguyen, H. H., Grigoriev, I. V., Wemmer, D. E., and Kim, S. H. (2002) *J. Mol. Biol.* **319,** 421–431
32. Zhang, G., Dai, J., Wang, L., Dunaway-Mariano, D., Tremblay, L. W., and Allen, K. N. (2005) *Biochemistry* **44,** 9404–9416
33. Pirard, M., Matthijs, G., Heykants, L., Schollen, E., Grunewald, S., Jaeken, J., and van Schaftingen, E. (1999) *FEBS Lett.* **452,** 319–322
34. Bjursell, C., Erlandson, A., Nordling, M., Nilsson, S., Wahlstrom, J., Stibler, H., Kristiansson, B., and Martinsson, T. (2000) *Hum. Mutat.* **16,** 395–400
35. Matthijs, G., Schollen, E., Bjursell, C., Erlandson, A., Freeze, H., Imtiaz, F., Kjaergaard, S., Martinsson, T., Schwartz, M., Seta, N., Vuillaumier-Barrot, S., Westphal, V., and Winchester, B. (2000) *Hum. Mutat.* **16,** 386–394
36. Pirard, M., Collet, J. F., Matthijs, G., and Van Schaftingen, E. (1997) *FEBS Lett.* **411,** 251–254
37. Alton, G., Hasilik, M., Niehues, R., Panneerselvam, K., Etchison, J. R., Fana, F., and Freeze, H. H. (1998) *Glycobiology* **8,** 285–295
38. Kraulis, P. (1991) *J. Appl. Crystallogr.* **24,** 946–950
39. Potterton, E., McNicholas, S., Krissinel, E., Cowtan, K., and Noble, M. (2002) *Acta Crystallogr. Sect. D Biol. Crystallogr.* **58,** 1955–1957